Front. Agr. Sci. Eng. 2024, 11(4): 544–560 https://doi.org/10.15302/J-FASE-2024581

RESEARCH ARTICLE

Effects of canopy resistance parameterization on evapotranspiration partitioning and soil water contents in a maize field under a semiarid climate

Lianyu YU[1,2], Huanjie CAI[1,2], Delan ZHU[1,2], Yuhan LIU[1], Fubin SUN[1], Xiangxiang JI[1], Yijian ZENG[3], Zhongbo SU[3], La ZHUO (✉)[4]

1 College of Water Resources and Architectural Engineering, Northwest A&F University, Yangling 712100, China.
2 Key Laboratory of Agricultural Soil and Water Engineering in Arid Area of Ministry of Education, Northwest A&F University, Yangling 712100, China.
3 Faculty of Geo-Information Science and Earth Observation, University of Twente, Enschede 7522 NH, the Netherlands.
4 College of Soil and Water Conservation Science and Engineering, Northwest A&F University, Yangling 712100, China.

KEYWORDS

Field experiment, STEMMUS-ET model, root-zone water budget, Northwest China

Received March 12, 2024;
Accepted July 17, 2024.

Correspondence: zhuola@nwafu.edu.cn

GRAPHICAL ABSTRACT

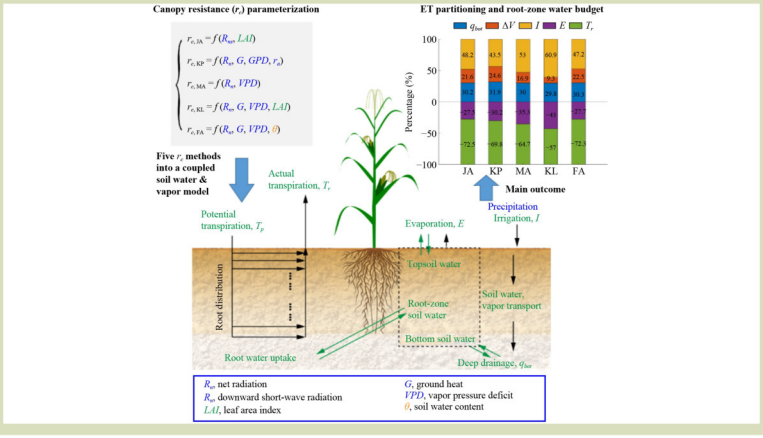

ABSTRACT

Different canopy resistance (r_c) parameterization has been used in land surface models to simulate actual evapotranspiration (ET_c) and soil hydraulic variable for crop fields. However, the influence of r_c parameterization on evapotranspiration (ET) partitioning and soil water dynamics has not been fully investigated with consideration of the coupled soil water and vapor physics. This study investigated the influential mechanisms of five r_c methods (viz., Jarvis, Katerji-Perrier, Massman, Kelliher-Leuning, and Farias) on ET partitioning and soil water contents in an irrigated maize field under a semiarid climate through a soil water and vapor transfer model. The Jarvis method presented the best ET results (R^2 = 0.86 and $RMSE$ = 0.71 mm·d^{-1}). Different r_c parameterization mainly altered the simulated amount of soil water contents, while not changed the response of soil water dynamics to irrigation events. By the integrated analysis of the ET partitioning and root-zone water budget, different r_c methods varied in the choice of the optimum irrigation water use strategies. This study identified the direct and indirect impacts of r_c on the ET

partitioning and emphasizes the necessity of both the ET partitioning and water supply sources in the decision-making for irrigation water management in semiarid regions.

1 Introduction

Soil water contents and crop evapotranspiration (ET), especially its partition into soil evaporation (E) and plant transpiration (T_r), are the key variables for the appropriate and efficient irrigation water management. Increasingly, the canopy resistance (r_c) has been reported as a crucial biophysical factor in explaining the variation of ET and ET partitioning[1–5]. Understanding the role of r_c in mediating the ET dynamics and soil water contents will be helpful for the agricultural irrigation water practice in semiarid regions.

ET estimation methods have been extensively studied for different ecosystems and climate[6–10]. Of which the Penman-Monteith (PM) model is widely used and has been verified applicable in various regions with different climate and vegetation cover[11–13]. Implementing the r_c and soil surface resistance, PM is extended to the two-component ET model and thus practical to partition ET into the physical component E and biophysical component T_r. ET partition was reported to be affected by soil factors (e.g., soil moisture[14,15]), plant factors (e.g., leaf area index (LAI), plant height[3,16]), and meteorological conditions (e.g., radiation, vapor pressure deficit[17,18]). The extent to which these factors control ET partitioning was found site-specific[3,19].

To better mimic the dynamics of r_c, researchers have contributed much efforts in portraying the r_c. Such work includes: (1) elaborating the influencing factors and their relative importance[20–25], (2) building up the empirical or mechanistic models[26–28], (3) making modifications or optimizations to improve the model performance, and (4) conducting model assessment and error analysis[29–32]. Various models have been developed, including the empirical models[26,30,33], semi-empirical models[31,34,35], optimum theory models[27,36], and mechanistic models[37,38]. Benefit from its simplicity and easy use, the empirical and semi-empirical models are still commonly used by land surface models or soil water models[39–41]. The model performance was found to vary with the temporal scale, growth stages, regions, and soil moisture conditions, which renders its necessity to conduct site-specific calibration and validation[30,42,43]. In addition, most of the validation work only covers the bulk simulation of ET[29,30,43], and lacks the further assessment of ET partitioning and soil water contents. This may hinder understanding of the role of r_c in affecting the efficient irrigation water management.

Soil water contents can be influenced by the water infiltration, surface soil E, root water extraction, soil water movement, and subsurface water percolation/recharge processes, of which soil water movement process is the central linkage among these processes. Soil water vapor transfer process, as it connects soil water and heat flow, has been recognized important in mimicking the dynamics of soil water movement, especially in arid or semiarid environments[44,45]. However, such process is seldom used in soil water models for the agricultural water resources management.

In this study, five different r_c parameterization (Jarvis, JA; Katerji-Perrier, KP; Farias, FA; Kelliher-Leuning, KL; Massman, MA) were used in the soil water model STEMMUS-ET[45–47], which can simulate the coupled liquid water, water vapor and heat flow in unsaturated soil, together with the root water uptake processes, to reproduce the dynamics of ET, soil E, T_r, and soil water content. Validated by the measurements collected in an irrigated summer maize field, the effect of various r_c parameterization on the ET partitioning and soil water contents were investigated. By integrating the analysis of root-zone water budget with ET partitioning, we also considered the role of r_c parameterization in decision-making for irrigation water management. The objectives of this study were: (1) to find the practical r_c parameterization for portraying ET, ET partitioning, and soil water dynamics over the maize field in semiarid regions; and (2) to investigate the influencing mechanisms of r_c parameterizations on ET partitioning, soil water dynamics, and the irrigation water management. Such results can help enrich understanding of the biophysical role of r_c in regulating ET partitioning and soil water dynamics and ultimately contribute to the improved irrigation water use for summer maize in the semiarid environment.

2 Materials and methods

2.1 Field experiment design

The field experiment was conducted at the Yangling Irrigation Experiment Station (34°17′ N, 108°04′ E, at an elevation of 521 m a.s.l.), at Northwest A&F University, Shaanxi Province of Northwest China. The experimental location is characterized as the semiarid to subhumid climate and drought-prone region. The mean annual air temperature is 12.9 °C, the mean annual precipitation is 630 mm, and the mean annual E is 1500 mm. The general soil type is silt clay loam with an average field capacity of 31.7 $m^3 \cdot m^{-3}$ and bulk density of 1.35 $g \cdot cm^{-3}$.

The field experiment was conducted in two large lysimeters under the mobile rainproof shelter (Fig. 1). The dimensions of the lysimeter system are 3 m × 2.2 m × 3 m (length, width, and depth). The weight readings were automatically recorded at the hourly interval with a precision of 139 g (i.e., 0.021 mm of water) for the weighing system and 1 g for the drainage system. To control the precipitation, the mobile rainproof shelter was installed above the lysimeters. Summer maize (cv. Wuke 2, a local cultivar) was sown on 23 June 2013 at a plant population of 40 plants within an area of 6.6 m^2 and harvested on 2 October 2013. During the experimental periods, the irrigation was applied when the soil water content dropped below a preset threshold (i.e., 60% of the field capacity). The level of irrigation was set to replace crop water consumed since the previous irrigation, as measured by the lysimeter. Two supplementary irrigations were applied in the early growing season (27 June and 3 July) to ensure uniform growth of the summer maize (the specific irrigation time and amount was shown in Table 1). Other agronomic practices were as use by local farmers.

2.2 Measurements and data collection

Meteorological data, including daily maximum and minimum air temperature, relative humidity, daily precipitation, sunshine duration and wind speed at 10 m above surface, were obtained from a standard weather station located inside the experimental site. Hourly values of air temperature, air humidity, and wind speed were generated from daily measurements using a trigonometric function[48], which has been demonstrated feasible in this region[45].

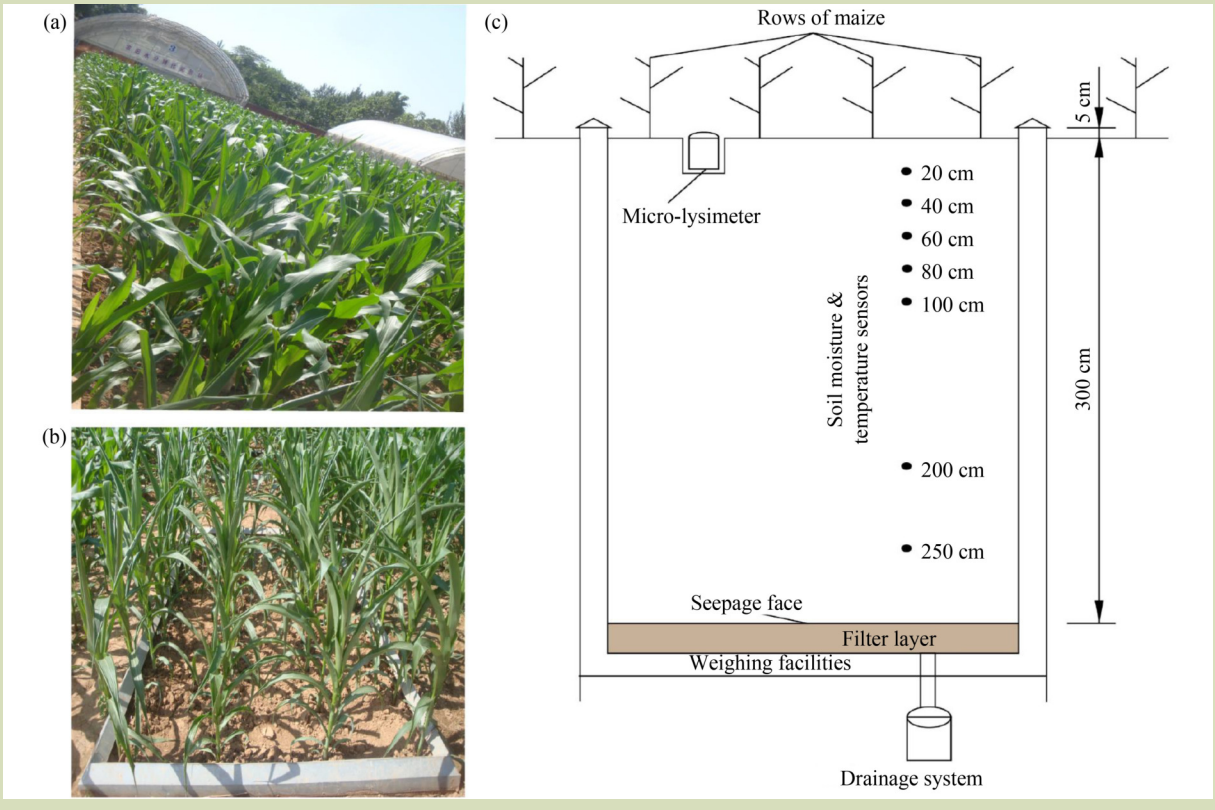

Fig. 1 The experimental site and lysimeter: (a) summer maize growing in the filed with a rainproof shelter, (b) summer maize growing in the lysimeter, and (c) the structure of the lysimeter.

Soil moisture were measured and recorded at the hourly interval using the pre-calibrated sensors (ThetaProbe ML2x, Delta-T Devices Ltd., Cambridge, UK), which were installed at depths of 20, 40, 60, 80, 100, 200, 225, and 250 cm. Soil water content at the topsoil layers was measured using the gravimetric method weekly. Hourly crop ET was calculated from the lysimeter weighted readings, which were further summed to obtain the daily ET values during the growing season. E was measured daily using the microlysimeters, which were placed between two crop rows. The use of the microlysimeter in this study area follows the recommendations by Kang et al.[49] and Wang et al.[50].

Leaf area and plant height were measured every 7–10 days after sowing, based on the average of at least three plant samples. LAI was calculated by the sum of the leaf area dividing the area of the plot. Leaf stomatal conductance measurements were conducted a few days (on sunny days) after irrigation using portable photosynthesis equipment (LI-6400, Li-Cor, Lincoln, NE, USA). Values were recorded from three functional leaves during 10:00–14:00 local time, when the stomatal conductance of summer maize reached its peak and remained steady[51]. The maximum rooting depth was about 1.2 m[45,52]. According the recommendations by Allen et al.[53], the crop stages or phenology were determined as in Table 1.

2.3 Soil water model

The STEMMUS-ET model[45–47] was used. The general structure of the used STEMMUS-ET model and the implementation of the different r_c parameterization in STEMMUS-ET are illustrated in Fig. 2. In this study, irrigation (I) and actual E were the top boundary fluxes, and the deep drainage (q_{bot}) was the bottom boundary flux of the STEMMUS-ET. The two-component PM method (Eqs. (5) and (6)), incorporating the r_c (Eqs. (11)–(16)) and actual soil surface resistance (Eq. (10)), was used to calculate the crop potential transpiration (T_p) and actual soil E, respectively. The actual T_r was then estimated from the root-density-weighed T_p, considering the reduction coefficient $\alpha(h)$ related to root-zone water conditions.

2.3.1 STEMMUS-ET

The governing equation of the liquid and vapor flow in STEMMUS-ET can be expressed as:

$$\frac{\partial}{\partial t}(\rho_L\theta_L+\rho_V\theta_V)=-\frac{\partial q_L}{\partial z}-\frac{\partial q_V}{\partial z}-S \quad (1)$$

where, ρ_L and ρ_V (kg·m^{-3}) are the density of liquid water and water vapor, respectively, θ_L and θ_V (m^3·m^{-3}) are the volumetric water content (liquid and vapor, respectively), z (m) is the vertical space coordinate; q_L and q_V (kg·m^{-2}·s^{-1}) are the soil liquid water and water vapor fluxes (positive upwards), respectively, and S (s^{-1}) is the sink term for the root water extraction.

The root water uptake term can be described as[54]:

$$S(h)=\alpha(h)S_p \quad (2)$$

Table 1 Crop growth stages and crop height for maize in 2013

Crop growth stage		Date	Crop height (m)	LAI (m^2·m^{-2})	Irrigation amount (mm)
Initial	Start	23 Jun.	0	0	
	Irrigation	26 Jun.			12.3
		2 Jul.			8.97
Crop development	Start	6 Jul.	0.22	0.47	
	Irrigation	13 Jul.			51.2
		22 Jul.			4.13
		2 Aug.			58.8
Middle season	Start	14 Aug.	1.65	5.24	
	Irrigation	16 Aug.			67.5
		9 Sep.			53.1
Late season	Start	14 Sep.	2.17	4.94	
	Harvest	2 Oct.	2.17	2.30	

Note: LAI, leaf area index.

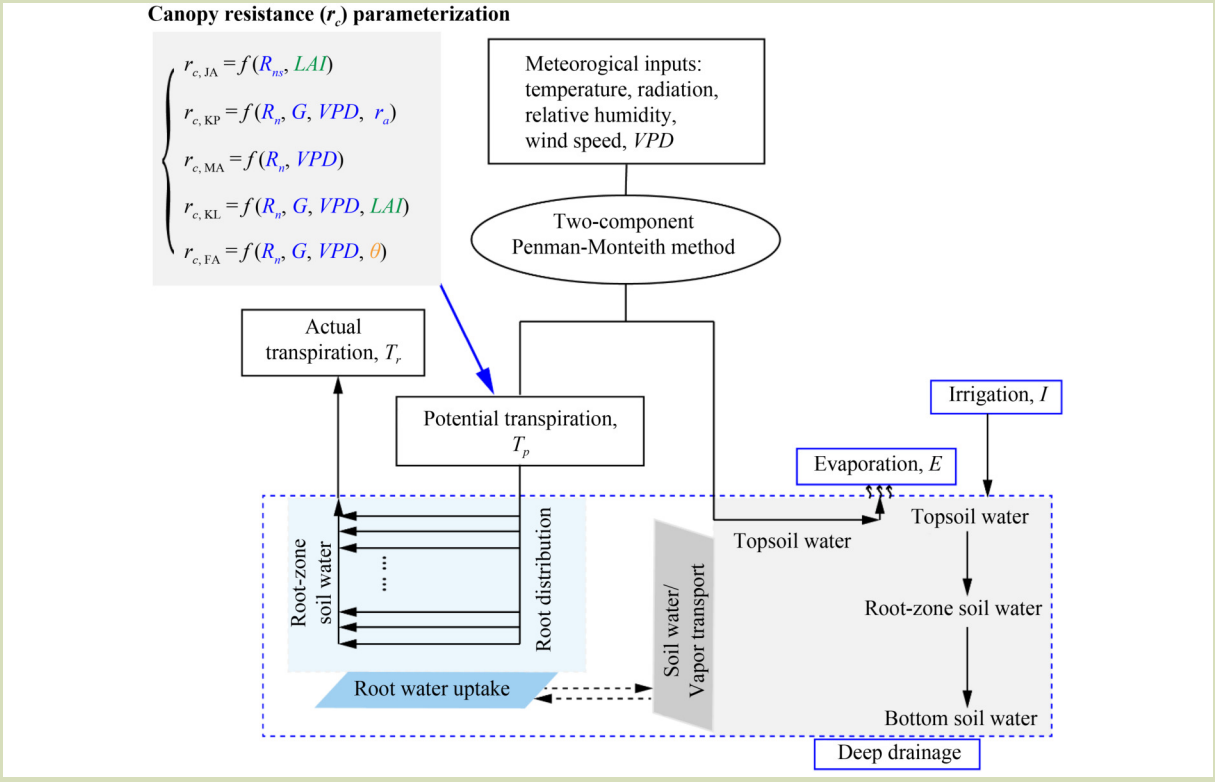

Fig. 2 Schematic of the STEMMUS-ET model with different canopy resistance parameterization. Blue module, i.e., root water uptake module, which used the potential transpiration as the input, and the actual transpiration and root water uptake sink term was calculated as the output. Gray module, i.e., soil water/vapor transport module, in which, soil water and vapor transfer among the topsoil, root-zone soil and bottom soil layers followed the Richards equation. Topsoil water is crucial in estimating actual soil evaporation. Bottom soil water was important in the calculation of the deep drainage water flux. Root-zone soil water was utilized to calculated the actual transpiration, which connects with the root water uptake module. R_{ns}, net solar radiation; *LAI*, leaf area index; *G*, soil ground heat flux; *VPD*, vapor pressure deficit; r_a, aerodynamic resisitance.

where, $\alpha(h)$ (dimensionless) is the reduction coefficient related to soil water potential.

$$\alpha(h) = \begin{cases} 0 & h \geqslant h_1 \\ \dfrac{h_1 - h}{h_1 - h_2} & h_1 > h \geqslant h_2 \\ 1 & h_2 > h \geqslant h_3(T_p) \\ \dfrac{h - h_4}{h_3(T_p) - h_4} & h_4 \geqslant h \\ 0 & h < h_4 \end{cases} \quad (3)$$

where, h (m) is the soil matric potential (negative values), h_1, h_2, h_3, and h_4 are the critical thresholds of soil matric potential. When soil matric potential h is higher than h_1, soil water content is high and root experiences oxygen deficiency, and when h is lower than h_4 (wilting point), root water uptake is set equal to zero. Between h_2 and h_3, root water uptake is maximal. Between h_1 and h_2 and between h_3 and h_4, a linear function is assumed. The parameter, h_3, is dependent on the water demand of the atmosphere and expressed as a function of the potential transpiration (T_p).

S_p (s^{-1}) is the potential root water uptake rate:

$$S_p = b(x) T_p \quad (4)$$

where, $b(x)$ is the normalized root water uptake distribution, as described in Šimůnek et al.[55], and T_p is the potential transpiration.

By incorporating actual soil resistance and r_c into the PM model, the actual soil E and T_p can be estimated simultaneously as:

$$T_p = \frac{\Delta R_n^c + \rho_a c_p \dfrac{(e_s - e_a)}{r_a}}{\lambda\left(\Delta + \gamma\left(1 + \dfrac{r_c}{r_a}\right)\right)} \quad (5)$$

$$E=\frac{\Delta(R_n^s-G)+\rho_a c_p\dfrac{(e_s-e_a)}{r_a}}{\lambda\left(\Delta+\gamma\left(1+\dfrac{r_s}{r_a}\right)\right)} \tag{6}$$

where, Δ (kPa·°C^{-1}) is the slope of the vapor pressure curve, γ (kPa·°C^{-1}) is the psychrometric constant. R_n^c and R_n^s (MJ·m^{-2}·d^{-1}) are the net radiation reaching the canopy surface and soil surface, respectively, G (MJ·m^{-2}·d^{-1}) is the soil heat flux density (set as 0.1 and 0.5 R_n during the daytime and night time, respectively), R_n (MJ·m^{-2}·d^{-1}) is the net radiation, ρ_a (kg·m^{-3}) is the air density, c_p (J·kg^{-1}·K^{-1}) is the specific heat capacity of air, λ (MJ·kg^{-1}) is the latent heat of vaporization, and e_a and e_s (kPa) are the actual and saturation vapor pressure, respectively. The difference between e_a and e_s is called *VPD* (vapor pressure deficit), r_a (s·m^{-1}) is the aerodynamic resistance, r_c (s·m^{-1}) is the canopy resistance, and r_s (s·m^{-1}) is the soil surface resistance.

Following Beer's law, the net radiation reaching the soil surface R_n^s and intercepted by the canopy surface R_n^c is calculated as:

$$R_n^s=R_n\exp(-k_Q LAI) \tag{7}$$

$$R_n^c=R_n(1-\exp(-k_Q LAI)) \tag{8}$$

where, k_Q is the extinction coefficient, and *LAI* (m^2·m^{-2}) is the leaf area index.

The aerodynamic resistance can be determined as:

$$r_a=\frac{\ln\left(\dfrac{z_m-d}{z_{om}}\right)\ln\left(\dfrac{z_h-d}{z_{oh}}\right)}{\mathrm{k}^2 u_z} \tag{9}$$

where, z_m and z_h (m) are the reference heights of the wind and humidity measurements, d (being 2/3 h_c) is the zero plane displacement, z_{om} (being 0.123 h_c) is the roughness length for the momentum transfer, z_{oh} (being 0.1 z_{om}) is the roughness length for the heat and vapor transfer, k is the Karman constant, u_z is the wind speed at the reference height, and h_c is the crop height.

The soil surface resistance was calculated following van de Griend and Owe[56]:

$$\begin{aligned} r_s &= \mathrm{r_{sl}}\ \theta_{\mathrm{top}}>\theta_{\min},\ h_{\mathrm{top}}>-10^3\mathrm{m} \\ r_s &= \mathrm{r_{sl}}\mathrm{e}^{a(\theta_{\min}-\theta_{\mathrm{top}})}\theta_{\mathrm{top}}\leqslant\theta_{\min},\ h_{\mathrm{top}}>-10^3\mathrm{m} \\ r_s &= \infty\ h_{\mathrm{top}}\leqslant-10^3\mathrm{m} \end{aligned} \tag{10}$$

where, $\mathrm{r_{sl}}$ (10 s·m^{-1}) is the resistance to molecular diffusion of the water surface, a (0.357) is the fitted parameter, θ_{top} is the topsoil water content, $\theta_{\min}$ is the minimum water content above which soil is able to deliver vapor at a potential rate, and h_{top} is the soil water potential at the top soil layer.

2.3.2 Canopy resistance parameterization

2.3.2.1 Jarvis type canopy resistance method

Considering the minimum leaf stomatal resistance, solar radiation and *LAI*, the Jarvis type canopy resistance $r_{c,\mathrm{JA}}$ can be expressed as[26,57]:

$$r_{c,\mathrm{JA}}=\frac{r_{l,\min}(a_1(a_2R_s+1))}{LAI_{\mathrm{eff}}(a_2R_s+a_3)} \tag{11}$$

where, $r_{l,\min}$ (s·m^{-1}) is the minimum leaf stomatal resistance, can be measured under the optimal growth conditions, R_s is the downward shortwave radiation, and LAI_{eff} is the effective leaf area index, which represents the leaves in the canopy that actively contribute to the heat and vapor transfer. a_1, a_2, and a_3 are the model parameters, referred from ECMWF[57].

2.3.2.2 Katerji-Perrier canopy resistance method

The Katerji-Perrier r_c method is described as[58]:

$$\frac{r_{c,\mathrm{KP}}}{r_a}=b_1\frac{r^*}{r_a}+b_2 \tag{12}$$

where, r_a (s·m^{-1}) is the aerodynamic resistance, which can be calculated as Eq. (9). b_1 and b_2 are the fitting parameters (as detailed in Table S1 (Supplementary materials)). r^* (s·m^{-1}) is the climatic resistance, can be expressed as:

$$r^*=\frac{\Delta+\gamma}{\Delta\gamma}\times\frac{\rho_a c_p VPD}{(R_n-G)} \tag{13}$$

2.3.2.3 Massman canopy resistance method

Massman[59] developed the r_c model as a function of photon flux density, vapor pressure deficit, and the maximum canopy conductance, i.e., the reciprocal of the minimum r_c, as:

$$\frac{1}{r_{c,\mathrm{MA}}}=g_{sm}\left(\frac{Q_p}{Q_p+c_1}\right)\left(\sqrt{\frac{c_2}{VPD}+c_3}\right) \tag{14}$$

where, g_{sm} (m·s^{-1}) is the maximum stomatal conductance, Q_p is the photosynthetically active radiation photon flux density, *VPD* is the vapor pressure deficit, and c_1, c_2, and c_3 are the model parameters (as detailed in Table S1).

2.3.2.4 Kelliher-Leuning canopy resistance method

The Kelliher-Leuning r_c method, considering the combined effect of plant leaf area, maximum stomatal conductance, and atmospheric radiation, vapor pressure deficit, was developed by Kelliher et al.[60] and further modified by Leuning et al.[28] as

$$\frac{1}{r_{c,\mathrm{KL}}}=\frac{g_{sm}}{k_Q}\ln\left(\frac{Q_h+Q_{50}}{Q_h\exp(-k_Q LAI)+Q_{50}}\right)\left(\frac{1}{1+VPD_a/VPD_{50}}\right) \tag{15}$$

where Q_h (taken as the half of incident solar radiation) is the

visible radiation flux density at the top of the canopy, Q_{50} and VPD_{50} are the visible radiation flux density and vapor pressure deficit when the stomatal conductance is the half of the maximum value, VPD_a is the actual vapor pressure deficit. The parameters used were as detailed in Table S1.

2.3.2.5 Farias canopy resistance method

Ortega-Farias et al.[61] proposed the r_c as the resistance to water transfer from the soil, via the plant, to the atmosphere, which is expressed as the function of climatic factors and available soil moisture.

$$r_{c,\mathrm{FA}} = r_i F(\theta)^{-1} = \frac{\rho_a c_p VPD}{\Delta (R_n - G)} F(\theta)^{-1} \tag{16}$$

where r_i (s·m^{-1}) is the modified meteorological resistance, $F(\theta)$ is the normalized soil moisture, can be determined as

$$F(\theta) = (\theta_{rt} - \theta_w)/(\theta_f - \theta_w) \tag{17}$$

where θ_{rt} (m^3·m^{-3}) is the averaged volumetric soil water content in the root zone; θ_w and θ_f (m^3·m^{-3}) are the volumetric water content at the wilting point and field capacity, respectively. Here $F(\theta)$ was set to 1, to avoid the duplicated consideration of soil water factors as with Eq. (3).

2.4 Model setup, calibration and validation

The STEMMUS-ET model was run with the fully coupled soil water, vapor, and heat flow. To accommodate the large lysimeter case, the soil profile was set as 3 m. It was further divided into 38 nodes with the relatively finer vertical discretization in the upper soil layers (0.25–5 cm at soil depth of 0–50 cm) than that in the lower soil layers (10–25 cm at soil depths of 60–300 cm).

The upper boundary was controlled by the soil E and irrigation water fluxes. The lower boundary was considered as the seepage face condition. The initial conditions for soil water and heat transport was determined by interpolating the measured soil moisture and temperature at the starting date.

Measurements in 2012 and 2013 were used to calibrate and validate the STEMMUS-ET model, respectively. The measurements and values from the relevant references were used as the initial values for the soil and plant parameters to run STEMMUS-ET[45]. Soil hydraulic parameters, crop growth parameters, and root water uptake related parameters were further calibrated by the trial and error using the measured soil water contents at different soil depths (i.e., 20, 40, 60, 80, and 100 cm), soil E, and ET. The empirical parameters in the r_c models were optimized using the genetic algorithm with the measured ET values in 2012 as the objective value. The detailed procedure can be found in Chen et al.[29]. The simulation results for 2012 were presented in the supplementary materials (Figs. S1–S2, Table S2). The calibrated soil and plant parameters used were as detailed in Table S1.

To assess the model performance, four commonly used performance metrics, i.e., the determination coefficient (R^2), index of agreement (d), root mean square error ($RMSE$), and model bias ($BIAS$) were used:

$$R^2 = \frac{\left[\sum_{i=1}^{n}\left(P_i - \overline{P}\right)\left(O_i - \overline{O}\right)\right]^2}{\sum_{i=1}^{n}\left(P_i - \overline{P}\right)^2 \sum_{i=1}^{n}\left(O_i - \overline{O}\right)^2} \tag{18}$$

$$d = 1 - \frac{\sum_{i=1}^{n}(P_i - O_i)^2}{\sum_{i=1}^{n}\left(\left|P_i - \overline{O}\right| + \left|O_i - \overline{O}\right|\right)^2} \tag{19}$$

$$RMSE = \sqrt{\frac{\sum_{i=1}^{n}(P_i - O_i)^2}{n}} \tag{20}$$

$$BIAS = \frac{\sum_{i=1}^{n}(P_i - O_i)}{n} \tag{21}$$

where, O_i, P_i, are the measured and model simulated values, $\overline{O}$ and $\overline{P}$ are the mean values of the measurements and model simulations, and n is the number of data points.

3 Results

3.1 Soil water dynamics

Figure 3 shows the comparison of dynamics of soil water contents simulated using the STEMMUS-ET model with the tested five r_c methods versus corresponding observations at different soil depths. In response to large irrigation events, soil water content at 20 cm increased sharply, while such response was moderated and greatly reduced in magnitude at deeper soil layers. The soil water content at 20 cm was generally well simulated by models with different r_c methods. The statistical analysis indicated that the model using the JA, KP, and FA r_c methods performed better relative to the other methods with a d-index higher than 0.78 and $RMSE$ lower than 0.0155 m^3·m^{-3} (Table 2). KL method presented the worst simulations with the largest $RMSE$, and lowest d-index. In deeper soil layers (40–100 cm), however, the dynamics of soil water content with irrigation simulated by different models were more variable than the observed values. The possible reason is that the soil moisture sensors might be not in close contact with the soils at deep soil layers (e.g., adjacent to macropores), making it difficult for STEMMUS-ET model to accurately reproduce the

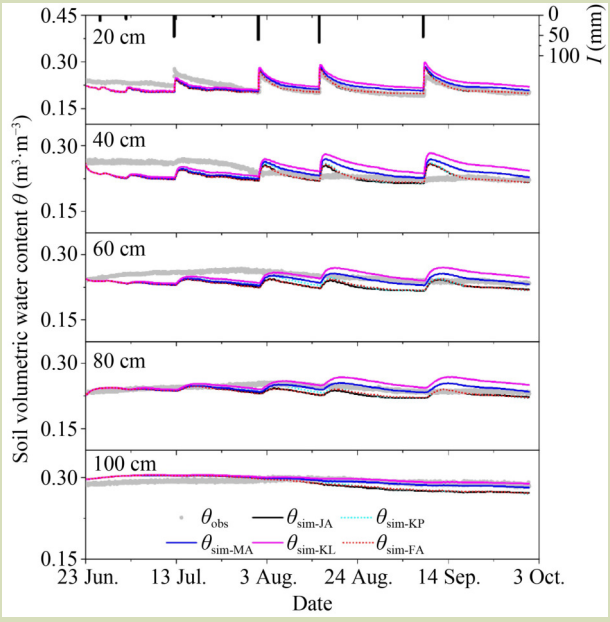

Fig. 3 Time series of measured and model simulated hourly soil water contents at different depths using the Jarvis (JA), Katerji-Perrier (KP), Massman (MA), Kelliher-Leuning (KL), and Farias (FA) canopy resistance methods.

measured soil moisture, since it did not take into account the effect of macropores on soil water and vapor transfer. The model performance was degraded with the increased soil depth, with the *d*-index values ranged from 0.0667 to 0.666, *RMSE* ranged from 0.0069 to 0.0288 $m^3 \cdot m^{-3}$, and *BIAS* ranged from –0.0186 to 0.0099 $m^3 \cdot m^{-3}$.

The difference in soil water content simulations among various r_c methods started from the second large irrigation event (2 August, in Fig. 3) and gradually enlarged with time. Model using the KL method overestimated the soil water content significantly compared with models using other r_c methods. The range of difference is 0.0075–0.0306 $m^3 \cdot m^{-3}$, which is comparable to the simulation errors (*RMSE* range from 0.0069 to 0.0288 $m^3 \cdot m^{-3}$).

3.2 Evapotranspiration and evapotranspiration partitioning

3.2.1 Daily evapotranspiration

Daily *ET* measured from the lysimetric system was used to assess the performance of models with different r_c methods

Table 2 Comparative statistics values of models with different canopy resistance parameterization for soil moisture in 2013

Models	Statistics	Soil moisture ($m^3 \cdot m^{-3}$)				
		20 cm	40 cm	60 cm	80 cm	100 cm
JA	*BIAS*	*–0.0077*	*–0.0110*	*–0.0186*	–0.0083	–0.0031
	d	0.799	0.541	0.478	0.527	*0.444*
	RMSE	0.0151	0.0207	0.0206	0.0115	*0.0116*
KP	*BIAS*	–0.0055	–0.0083	–0.0160	–0.0059	**–0.0020**
	d	**0.827**	**0.566**	**0.549**	**0.666**	0.482
	RMSE	**0.0139**	**0.0195**	0.0179	0.0093	0.0111
MA	*BIAS*	**–0.0001**	**–0.0015**	–0.0091	**0.0011**	0.0022
	d	0.691	0.216	0.394	0.552	**0.580**
	RMSE	0.0174	0.0235	**0.0158**	**0.0077**	**0.0069**
KL	*BIAS*	0.0076	0.0079	**0.0001**	*0.0099*	*0.0055*
	d	*0.567*	*0.0667*	*0.148*	*0.356*	0.519
	RMSE	*0.0219*	*0.0288*	0.0169	*0.0148*	0.0071
FA	*BIAS*	–0.0076	–0.0109	–0.0184	–0.0081	–0.0028
	d	0.787	0.516	0.474	0.539	0.463
	RMSE	0.0155	0.0212	*0.0206*	0.0111	0.0110

Note: JA, Jarvis; KP, Katerji-Perrier; MA, Massman; KL, Kelliher-Leuning; FA, Farias. Values with bold fonts and italic fonts indicate the significant and non-significant statistical performance, respectively.

(Fig. 4). In response to the irrigation, *ET* increased rapidly at the initial growth stage (peak value of 4.73 mm·d^{-1}, Fig. 4(a)), mainly due to the increased soil *E*. Such response was more significant in magnitude during the crop development and middle growth stages as the more efficient transpired water loss than the evaporated water loss following the irrigation events (peak value of 9.51 mm·d^{-1}). As the fraction of transpiration decreased at the late growing stage, the response of *ET* to

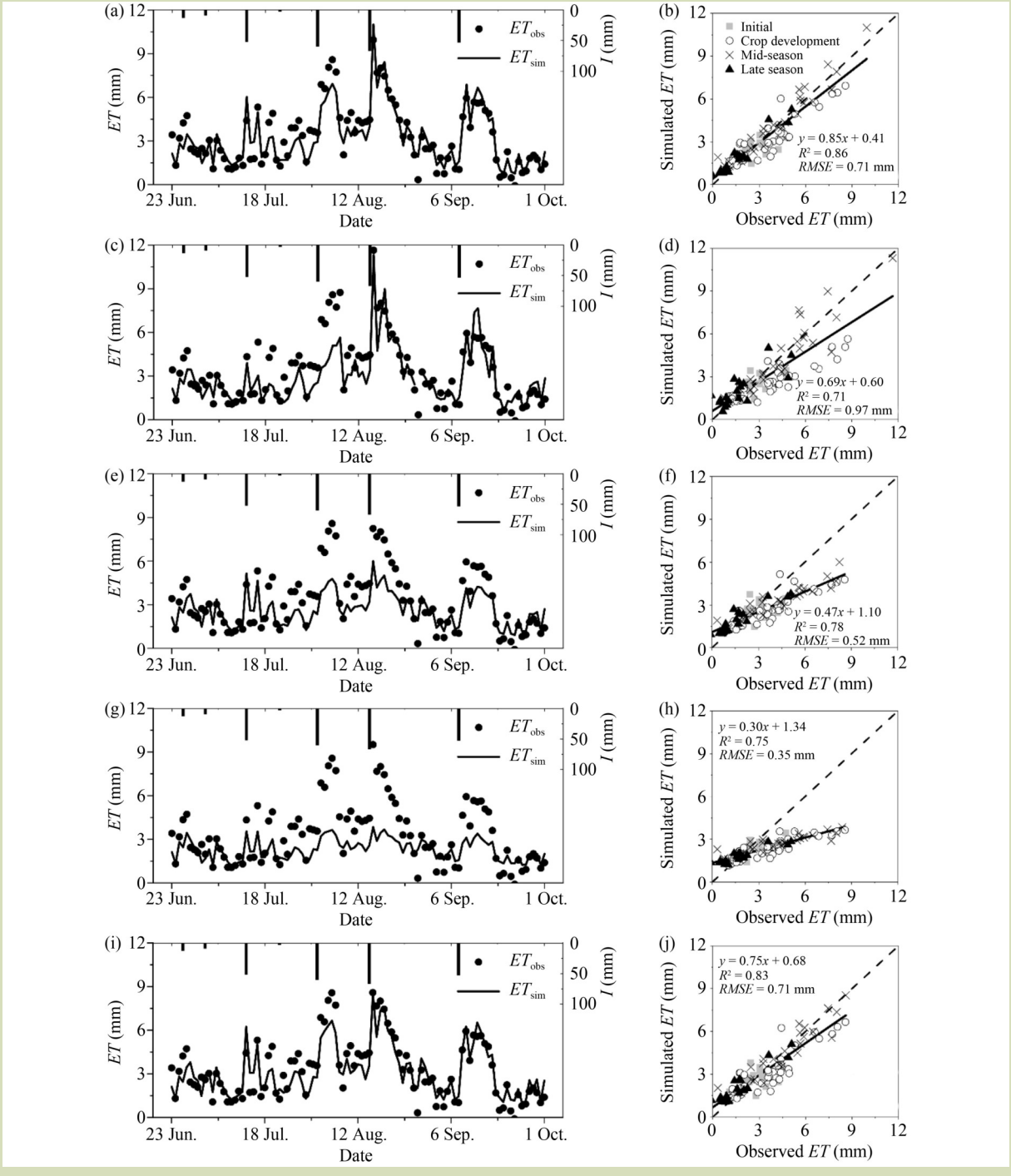

Fig. 4 Daily variation in and the correlation relationship between observed evapotranspiration (*ET*) and simulated *ET*, based on the (a) and (b) Jarvis (JA), (c) and (d) Katerji-Perrier (KP), (e) and (f) Massman (MA), (g) and (h) Kelliher-Leuning (KL), (i) and (j) Farias (FA) methods. *I*, irrigation.

irrigation events decreased gradually and was comparable to that of the initial stage (peak value of 5.09 mm·d^{-1}). Models with five r_c methods produced the different *ET* values ($p < 0.05$, Fig. S3), especially differed in the response of crop water consumption to the applied irrigation events. Except the underestimation of *ET* at the initial growth stage, JA and FA methods yielded an acceptable estimation against daily *ET* observations. KP method underestimated such response at the initial and crop development growth stages, while MA and KL methods yielded the underestimation at the initial, crop development, middle season and late season growth stages.

The PM model with five r_c methods presented an underestimation of crop *ET* during the initial stage, probably due to that the soil *E* was underestimated under low *LAI* (Fig. 4). Other than that, JA method well simulated the dynamics of daily *ET* in response to the applied irrigation events, with the highest R^2 (Fig. 4(a)). FA method presented the slightly worse simulations with the R^2 of 0.83 and *RMSE* of 0.71 mm·d^{-1}. Statistical analysis indicated that the KP method had the weakest correlation against the daily *ET* observations with the R^2 lower than 0.75.

Previous studies have reported the applicability of JA methods in various regions with different ecosystems[29,30,42,62]. Li et al.[30] reviewed various r_c parameterization and assessed their relative merits. The weak performance in *ET* simulations was reported for the JA method under low *LAI*, under which the role of soil resistance cannot be omitted. Li et al.[30] developed the coupled surface resistance scheme, which takes into account the soil and plant components, and obtained an acceptable *ET* result. Similarly, Chen et al.[29] found that the original single source PM model with the JA method cannot reproduce the observed *ET* while an acceptable performance was achieved with the SW model. By independently taking into account the effect of soil resistance, the two-component PM model with the JA method successfully simulated the daily *ET* dynamics in our study. This confirms the highlights by Chen et al.[29] and Li et al.[30] that the soil factors should be considered in r_c methods when the canopy is sparse.

For the KP method, an underestimation was found at the initial and crop development growth stages, and an overestimation was found at the middle season growth stages resulting in the large discrepancies, i.e., highest *RMSE* and lowest R^2 at the daily time scale. This could be due to that KP method only considers the meteorological factors and lack of the plant physiological constraints. In contrast, the MA method mostly underestimated the *ET* values, although with an acceptable correlation ($R^2 = 0.78$). The similar underestimation of *ET* was found with KL method. Nevertheless, KL method presents acceptable correlation and lowest *RMSE* ($R^2 = 0.75$ and *RMSE* = 0.35 mm·d^{-1}) indicating the potential advantages of taking into account the crop factors. For the FA method, the results were pleasing, particularly as this method requires no parameter calibration. This agrees with the results from Chen et al.[29] that the FA method provided acceptable *ET* simulations, indicating its potential application for the estimation of maize *ET* in this region.

3.2.2 Soil evaporation

Figure 5 shows the performance of the models using the JA, KP, MA, KL, and FA r_c methods in mimicking the dynamics of soil *E* measured by the microlysimeters. Models with different r_c methods produced the similar soil *E* dynamics and captured the increase of *E* in response to the applied irrigation events. The cumulative errors rose rapidly mainly at the middle and late crop growth stages (Fig. 5(b)). These discrepancies can be explained by the representativeness bias of soil *E* measured by microlysimeters under conditions of the crop growth[63,64]. Since the microlysimeter does not take into account the soil water loss due to crop root water extraction, the observed soil *E* may have been higher than the actual soil *E*. The difference

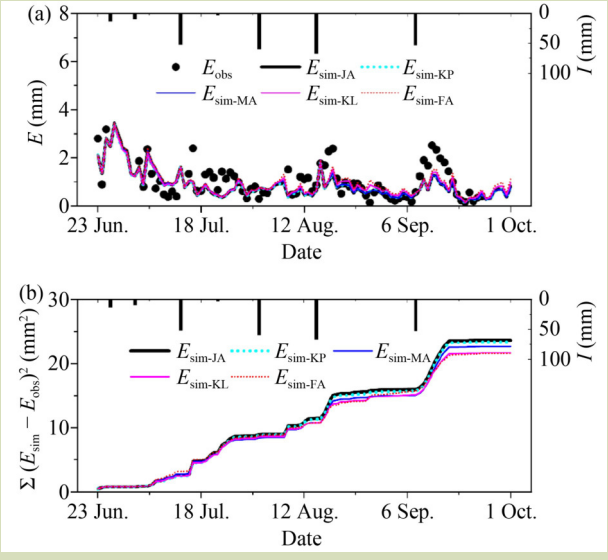

Fig. 5 Time series of (a) the observed and simulated daily soil evaporation (*E*), and (b) the cumulative errors ($\sum(E_{sim} - E_{obs})^2$), using the Jarvis (JA), Katerji-Perrier (KP), Massman (MA), Kelliher-Leuning (KL), and Farias (FA) canopy resistance methods. *I*, irrigation.

between models with different r_c methods (JA and KP, versus MA, versus KL and FA) started from 16 August (in Fig. 5) and increased rapidly after the main irrigation events. The overall maximum cumulative difference was about 12.8 mm, i.e., 0.12 mm·d^{-1}, which is lower than the model estimation errors, with *RMSE* values ranged from 0.46 to 0.48 mm·d^{-1}.

3.2.3 Evapotranspiration partitioning

To further elaborate how the water is consumed during the growing season, Table 3 presents the crop stage-specific *ET*, *E*, T_r, and evaporation fraction (*EF* being *E*/*ET*). Crop development and middle season stages are the two growth stages with higher water consumption rate than the initial and late season stages, with the daily average *ET* of 3.61 and 4.03 mm·d^{-1} versus 2.68 and 1.74 mm·d^{-1}. All models presented the similar seasonal variation patterns, the water consumption started to increase from the initial growth stage, developed rapidly at the crop development stage, reached the maximum at the middle season stage and decreased at the late season stage.

At the initial growth stage, soil *E* was dominant. With the different crop transpiration estimates, *EF* ranged from 77.4% to 92.8% using models with five r_c methods. As the crop development, the fraction of soil *E* decreased and reached its minimum at the middle season stage with the range of 17.3% to 34.4%, which indicated that crop transpiration was the primary contribution to the crop water consumption. At the late season growth stage, the proportion of soil *E* increased a little bit, which was most likely due to the decrease of crop transpiration as the crop senesced.

The variation ranges of *EF* due to different r_c methods were maximum at the initial and late season growth stages as the change of crop transpiration is large, which indicated that the effect of r_c parameterization on *EF* was more significant at these two crop growth stages.

Table 3 The actual evapotranspiration (ET_c), and model simulated soil evaporation (*E*), transpiration (T_r), evapotranspiration (*ET*), and evaporation fraction (*EF*) for each development stage of maize using the Jarvis (JA), Katerji-Perrier (KP), Massman (MA), Kelliher-Leuning (KL), and Farias (FA) canopy resistance methods

Crop stage		Initial	Crop development	Middle season	Late season	All
Observed	ET_c (mm)	37.5	141	125	31.2	335
JA	*E* (mm)	29.0	28.6	22.6	8.71	89.0
	T_r (mm)	5.21	94.5	108	27.0	235
	ET (mm)	34.2	123	131	35.7	324
	EF (%)	84.8	23.3	17.3	24.4	27.5
KP	*E* (mm)	28.9	30.3	23.1	8.61	90.9
	T_r (mm)	4.84	71.2	105	28.4	210
	ET (mm)	33.8	102	124	37.0	296
	EF (%)	85.7	29.8	18.6	23.3	30.7
MA	*E* (mm)	28.4	29.8	26.0	10.3	94.6
	T_r (mm)	7.58	71.4	69.6	25.2	174
	ET (mm)	36.0	101	95.6	35.5	268
	EF (%)	78.9	29.5	27.2	29.1	35.3
KL	*E* (mm)	29.4	31.9	28.1	11.8	101
	T_r (mm)	2.30	57.7	53.5	20.3	134
	ET (mm)	31.7	89.6	81.6	32.0	235
	EF (%)	92.8	35.6	34.4	36.7	43.1
FA	*E* (mm)	28.3	28.3	23.1	8.63	88.3
	T_r (mm)	8.28	92.5	100	29.8	231
	ET (mm)	36.6	121	123	38.4	319
	EF (%)	77.4	23.4	18.8	22.5	27.7

3.3 Root-zone water budget components

The effect of different r_c methods on the root-zone water budget components, including q_{bot}, ΔV, I, E, and T_r, is illustrated in Fig. 6. Constraint by the structure of the lysimetric system, the surface runoff and lateral water flux can be neglected. Thus, the lysimetric system can be used to understand how the incoming water supply contributes to the crop water consumption. The applied irrigation water is the solely incoming water flux, which experiences the infiltration, soil E, soil water transport and redistribution, and root water uptake processes, then affects the bottom water flux. E and T_r are the two kind of water consumption. As the applied irrigation water amount was less than the crop water consumption, other water supply sources (ΔV and q_{bot}) also contributed.

All models indicated that *ET* was mostly consumed by crop transpiration, with the minimum fraction of 57.0% estimated by the KL method and the maximum fraction of 72.5% by the JA method. Compared to crop transpiration, soil E exhibited a compensatory contribution to *ET*. As for the three water supply sources (I, q_{bot}, and ΔV), the contribution of bottom water flux q_{bot} to *ET* is similarly simulated by five different models (small variation from 29.8% to 31.9%), which means that the steady contribution from the other two water supply sources (ΔV and I) to *ET*. The relative magnitude of the change of ΔV among five r_c methods is similar to that of crop transpiration, while contrary to that of incoming I. This implicitly indicated that the change of root-zone soil water storage is closely related to crop transpiration.

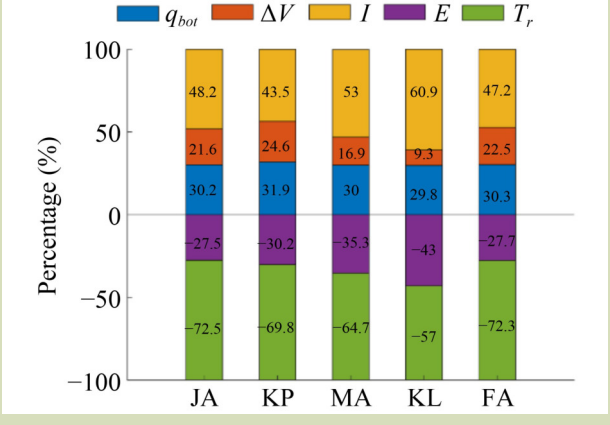

Fig. 6 Model estimated water budget components for the root zone, using the Jarvis (JA), Katerji-Perrier (KP), Massman (MA), Kelliher-Leuning (KL), and Farias (FA) canopy resistance methods. q_{bot}, bottom water flux; ΔV, change of soil water storage; I, irrigation; E, soil evaporation; and T_r, crop transpiration.

Given that the contribution of bottom water flux to *ET* was consistent among different r_c methods, their effect mainly functions in the root-zone soil layers and had minimum influence on the bottom soil layers in the experimental location. The effect of different r_c methods on root-zone water budget components is mainly twofold. First, it affects the way how the water is consumed. Models using different r_c methods presented various crop transpiration simulations, thus altered the *ET* partitioning strategies. Second, it alters the relative contribution of water supply sources. The greater the crop transpiration, the greater the depletion of root-zone ΔV and less utilization of I. This could be due to the fact that the recharge of the applied irrigation water cannot quickly replenish the root-zone soil water. Irrigation affects the water conditions primarily at topsoil layers while the root water uptake process is dominant at subsurface root-zone soil layers.

4 Discussion

4.1 Role of canopy resistance parameterization in modeling soil water dynamics

Soil water conditions are usually regarded as an important factor controlling r_c/conductance. It is reported that soil moisture can directly affect the r_c, but also can interact with other environmental factors and co-regulate the plant physiologic response, thus shaping the environmental controlling mechanisms of r_c[23,65]. Our results, conversely, investigated the effect of r_c parameterization on the model interpreting of soil water content dynamics. Results indicated that it exhibited the direct effects on the crop transpiration, then affected the root water uptake processes and altered root-zone soil water content. This is evidenced in Fig. 3, with greater transpiration simulated by the JA and FA methods, and greater depletion of soil moisture from the root-zone soil layers. However, it can affect the surface soil water content, via the vertical soil water movement and water redistribution processes. Such influence is not that significant, as indicated by the small difference in the simulated soil E (Fig. 5). Different r_c parameterization mainly altered the magnitude of soil water content, while not changing the response of soil water dynamics to irrigation events. This is consistent with the results from Yu et al.[45] that the similar trend but different in the magnitude of soil water content were given by models using different *ET* methods.

4.2 Role of canopy resistance parameterization in modeling evapotranspiration partitioning

ET partitioning describes how the water is used via the abiotic and biotic pathways, which is important for the understanding of land surface-atmosphere interactions and efficient irrigation management. Previous studies have mostly focused on the controlling factors on *ET* and *ET* partitioning, and found that r_c, which is a function of *LAI*, solar radiation and soil water availability, give a better explanation[1–3]. In this study, we investigated the effect of r_c parameterization on the model-portrayed *ET* partitioning. Primarily, r_c parameterization affects the transpiration and thus the *ET* partitioning, especially at the initial and late season growth stages. However, it can affect soil water redistribution and surface soil water condition, which then slightly alters the soil *E* (as evident in Fig. 5), resulting in the different *EF* values (Table 3).

4.3 Implications for the irrigation water management

We coupled the analysis of root-zone water budget with *ET* partitioning to examine how r_c parameterization affects the decision-making about irrigation water management. Crop transpiration, which links to the photosynthesis processes and biomass/yield formation, is generally considered to be the effective use of water, while soil *E* is regarded as a wasteful loss of water[66]. It is thus crucial to reduce the soil *E* and increase the crop transpiration, for water-saving actions in semiarid and arid environments. From the water supply perspective, improving irrigation water use efficiency and reducing ΔV are regarded as the best practices for the sustainable agriculture water conservation. Coupling the these, we proposed an integrated irrigation water use efficiency index, *IUE*, defined as $(I/\Delta V)/(E/ET)$ to synthetically assess the efficiency of water use in semiarid and arid regions. The higher values mean the more efficient the use of irrigation water and the smaller proportion of water loss as soil *E*, indicating the better irrigation water conservation management.

As shown in Fig. 7, models with different r_c methods presented various values of *IUE*, with the KL method being the highest score and the KP method having the lowest value. If we accept the simulations provided by the KL method, all other methods would provide relatively conservative guidance on agriculture water management. This is different from the suggestions based only on *ET* partitioning results, where the JA method tended to give the best water use practice due to its highest crop transpiration consumption (Fig. 6).

Fig. 7 Integrated irrigation water use efficiency (*IUE*) index estimated using the model with the Jarvis (JA), Katerji-Perrier (KP), Massman (MA), Kelliher-Leuning (KL), and Farias (FA) canopy resistance methods.

4.4 Limitations and outlook

The current work investigated the role of r_c parameterization in modeling the *ET* partitioning and soil water dynamics, and further elaborated the implications on the irrigation water management. Five r_c methods were incorporated into a detailed soil water and vapor coupled model. Several assumptions were adopted in our work. First, the used parameters in the r_c methods were assumed the same throughout the crop growth period. Such limitations in parameters, i.e., a single set of parameters for the whole growing season, resulted in the variation in performance in the *ET* estimates at different crop growth stages (Fig. 4). Second, the model structure and parameters of soil surface resistance parameterization were assumed to inevitably introduce great and inscrutable uncertainties if soil and canopy surface resistance were estimated separately. Thus, in this study, we adopted the commonly used *big-leaf* hypothesis with the PM model to estimate the r_c. The measured *ET* was used in PM model to inversely derive the surface resistance, which was assumed to be the r_c (neglect the effect of soil *E*). Such an assumption appears questionable under the partial canopy stage (Fig. 4). Nevertheless, it reliably reproduced the role of r_c under the full canopy stage (when *ET* is large and its temporal coverage was about 75% in this study). In the future work, the segmented r_c parameter calibration and detailed investigation of the relationship between the r_c and the mean surface resistance needs to be undertaken to improve the *ET* model performance and reduce the simulation uncertainties[30,67,68].

5 Conclusions

The performance of five r_c parameterization was validated and its influence on the *ET* partitioning and soil water content were further elaborated over an irrigated maize field in a semiarid environment. Models with five r_c methods can reproduce the temporal dynamics of *ET*, soil *E* and soil water content, and their response to applied irrigation events, but differed in the magnitude. The JA method provided the most acceptable *ET* estimates on the basis of PM equation with the explicit consideration of the soil component. The FA method was found to have the potential to provide the reasonable *ET* estimates in this region. Two possible influencing mechanisms on *ET* partitioning were identified: (1) the direct effect of r_c parameterization on the transpiration estimations, root water uptake process and root-zone water content, and (2) the indirect effect through its influence on the water redistribution process, as it can alter surface soil water content then the soil *E*. The simulated *ET* partitioning and root-zone water budget analysis demonstrated that different r_c methods varied in the estimation of both the contribution of water supply sources and water consumption strategies. Various r_c methods differ in their choice of the optimum irrigation water use strategy, based on such simulations, that different from the outcome based solely on *ET* partitioning analysis. It is suggested that both the *ET* partitioning and water supply sources analysis should be considered when making decisions for water management in the irrigated agricultural regions in semiarid environments.

Supplementary materials

The online version of this article at https://doi.org/10.15302/J-FASE-2024581 contains supplementary materials (Figs. S1–S3; Tables S1–S2).

Acknowledgements

This research was supported by Chinese Universities Scientific Fund (Z1090122048), Cyrus Tang Foundation, Shaanxi Province Science Foundation for Youths (2024JC-YBQN-0531), and Special Project for the Investigation of Basic Resources of Ministry of Science and Technology, China (2022FY101602).

Compliance with ethics guidelines

Lianyu Yu, Huanjie Cai, Delan Zhu, Yuhan Liu, Fubin Sun, Xiangxiang Ji, Yijian Zeng, Zhongbo Su, and La Zhuo declare that they have no conflicts of interest or financial conflicts to disclose. This article does not contain any studies with human or animal subjects performed by any of the authors.

REFERENCES

1. Bu J, Gan G, Chen J, Su Y, García M, Gao Y. Biophysical constraints on evapotranspiration partitioning for a conductance-based two source energy balance model. *Journal of Hydrology*, 2021, **603**: 127179
2. Jia X, Zha T S, Gong J N, Wu B, Zhang Y Q, Qin S G, Chen G P, Feng W, Kellomäki S, Peltola H. Energy partitioning over a semi-arid shrubland in northern China. *Hydrological Processes*, 2016, **30**(6): 972–985
3. Wang P, Li X Y, Wang L, Wu X, Hu X, Fan Y, Tong Y. Divergent evapotranspiration partition dynamics between shrubs and grasses in a shrub-encroached steppe ecosystem. *New Phytologist*, 2018, **219**(4): 1325–1337
4. Forster M A, Kim T D H, Kunz S, Abuseif M, Chulliparambil V R, Srichandra J, Michael R N. Phenology and canopy conductance limit the accuracy of 20 evapotranspiration models in predicting transpiration. *Agricultural and Forest Meteorology*, 2022, **315**: 108824
5. Bu J, Gan G, Chen J, Su Y, Yuan M, Gao Y, Domingo F, López-Ballesteros A, Migliavacca M, El-Madany T S, Gentine P, Xiao J, Garcia M. Dryland evapotranspiration from remote sensing solar-induced chlorophyll fluorescence: constraining an optimal stomatal model within a two-source energy balance model. *Remote Sensing of Environment*, 2024, **303**: 113999
6. Dickinson R E, Henderson-Sellers A, Rosenzweig C, Sellers P J. Evapotranspiration models with canopy resistance for use in climate models, a review. *Agricultural and Forest Meteorology*, 1991, **54**(2-4): 373–388
7. Ershadi A, Mccabe M F, Evans J P, Wood E F. Impact of model structure and parameterization on Penman-Monteith type evaporation models. *Journal of Hydrology*, 2015, **525**: 521–535
8. Federer C A, Vörösmarty C, Fekete B. Intercomparison of methods for calculating potential evaporation in regional and global water balance models. *Water Resources Research*, 1996, **32**(7): 2315–2321
9. Rana G, Katerji N, Lazzara P, Ferrara R M. Operational determination of daily actual evapotranspiration of irrigated

tomato crops under Mediterranean conditions by one-step and two-step models: multiannual and local evaluations. *Agricultural Water Management*, 2012, **115**: 285–296

10. Stannard D I. Comparison of Penman-Monteith, Shuttleworth-Wallace, and Modified Priestley-Taylor Evapotranspiration Models for wildland vegetation in semiarid rangeland. *Water Resources Research*, 1993, **29**(5): 1379–1392
11. Shuttleworth W J, Wallace J S, 0, 0. Calculating the water requirements of irrigated crops in Australia using the matt-shuttleworth approach. *Transactions of the ASABE*, 2009, **52**(6): 1895–1906
12. Zhou M C, Ishidaira H, Takeuchi K. Estimation of potential evapotranspiration over the Yellow River basin: reference crop evaporation or Shuttleworth-Wallace. *Hydrological Processes*, 2007, **21**(14): 1860–1874
13. Zhao W Z, Ji X B, Kang E S, Zhang Z H, Jin B W. Evaluation of Penman-Monteith model applied to a maize field in the arid area of Northwest China. *Hydrology and Earth System Sciences*, 2010, **14**(7): 1353–1364
14. Cui J, Tian L, Wei Z, Huntingford C, Wang P, Cai Z, Ma N, Wang L. Quantifying the controls on evapotranspiration partitioning in the highest alpine meadow ecosystem. *Water Resources Research*, 2020, **56**(4): e2019WR024815
15. Scott R L, Knowles J F, Nelson J A, Gentine P, Li X, Barron-Gafford G, Bryant R, Biederman J A. Water availability impacts on evapotranspiration partitioning. *Agricultural and Forest Meteorology*, 2021, **297**: 108251
16. Liu C, Zhang X, Zhang Y. Determination of daily evaporation and evapotranspiration of winter wheat and maize by large-scale weighing lysimeter and micro-lysimeter. *Agricultural and Forest Meteorology*, 2002, **111**(2): 109–120
17. Xu J, Wu B, Ryu D, Yan N, Zhu W, Ma Z. Quantifying the contribution of biophysical and environmental factors in uncertainty of modeling canopy conductance. *Journal of Hydrology*, 2021, **592**: 125612
18. Wang H, Guan H, Deng Z, Simmons C T. Optimization of canopy conductance models from concurrent measurements of sap flow and stem water potential on Drooping Sheoak in South Australia. *Water Resources Research*, 2014, **50**(7): 6154–6167
19. Li X, Gentine P, Lin C, Zhou S, Sun Z, Zheng Y, Liu J, Zheng C. A simple and objective method to partition evapotranspiration into transpiration and evaporation at eddy-covariance sites. *Agricultural and Forest Meteorology*, 2019, **265**: 171–182
20. Komatsu H, Kang Y, Kume T, Yoshifuji N, Hotta N. Transpiration from a Cryptomeria japonica plantation, part 2: responses of canopy conductance to meteorological factors. *Hydrological Processes*, 2006, **20**(6): 1321–1334
21. Yu L, Cai H, Zheng Z, Li Z, Wang J. Towards a more flexible representation of water stress effects in the nonlinear Jarvis model. *Journal of Integrative Agriculture*, 2017, **16**(1): 210–220
22. Flo V, Martínez-Vilalta J, Granda V, Mencuccini M, Poyatos R. Vapour pressure deficit is the main driver of tree canopy conductance across biomes. *Agricultural and Forest Meteorology*, 2022, **322**: 109029
23. Niu X, Chen Z, Pang Y, Liu X, Liu S. Soil moisture shapes the environmental control mechanism on canopy conductance in a natural oak forest. *Science of the Total Environment*, 2023, **857**: 159363
24. Cai G, König M, Carminati A, Abdalla M, Javaux M, Wankmüller F, Ahmed M A. Transpiration response to soil drying and vapor pressure deficit is soil texture specific. *Plant and Soil*, 2022, **500**(1–2): 129–145
25. Chen S, Zhang Z, Chen Z, Xu H, Li J. Responses of canopy transpiration and conductance to different drought levels in Mongolian pine plantations in a semiarid urban environment of China. *Agricultural and Forest Meteorology*, 2024, **347**: 109897
26. Jarvis P G. Interpretation of the variations in leaf water potential and stomatal conductance found in canopies in the field. *Philosophical Transactions of the Royal Society of London. Series B, Biological Sciences*, 1976, **273**(927): 593–610
27. Medlyn B E, Duursma R A, Eamus D, Ellsworth D S, Colin Prentice I, Barton C V M, Crous K Y, De Angelis P, Freeman M, Wingate L. Reconciling the optimal and empirical approaches to modelling stomatal conductance. *Global Change Biology*, 2011, **17**(6): 2134–2144
28. Leuning R, Zhang Y Q, Rajaud A, Cleugh H, Tu K. A simple surface conductance model to estimate regional evaporation using MODIS leaf area index and the Penman-Monteith equation. *Water Resources Research*, 2008, **44**(10): W10419
29. Chen X, Yu L, Cui N, Cai H, Jiang X, Liu C, Shu Z, Wu Z. Modeling maize evapotranspiration using three types of canopy resistance models coupled with single-source and dual-source hypotheses—A comparative study in a semi-humid and drought-prone region. *Journal of Hydrology*, 2022, **614**: 128638
30. Li S, Zhang L, Kang S, Tong L, Du T, Hao X, Zhao P. Comparison of several surface resistance models for estimating crop evapotranspiration over the entire growing season in arid regions. *Agricultural and Forest Meteorology*, 2015, **208**: 1–15
31. Yu Q, Zhang Y, Liu Y, Shi P. Simulation of the stomatal conductance of winter wheat in response to light, temperature and CO_2 changes. *Annals of Botany*, 2004, **93**(4): 435–441
32. Yan H, Zhou Y, Zhang J, Wang G, Zhang C, Yu J, Li M, Zhao S, Deng S, Liang S, Jiang J, Ni Y. Parametrization of canopy resistance and simulation of latent heat fluxes for typical crops in southern Jiangsu Province. *Transactions of the Chinese Society of Agricultural Engineering*, 2022, **38**(9): 101–107 (in Chinese)
33. Shao W, Li M, Su Y, Gao H, Vlček L. A modified Jarvis model to improve the expressing of stomatal response in a beech forest. *Hydrological Processes*, 2023, **37**(8): e14955
34. Leuning R. Modelling stomatal behaviour and photosynthesis of *Eucalyptus grandis*. *Australian Journal of Plant Physiology*, 1990, **17**(2): 159–175
35. Ball J T, Woodrow I E, Berry J A. A Model predicting stomatal conductance and its contribution to the control of

photosynthesis under different environmental conditions. In: Biggins J, ed. Progress in Photosynthesis Research: Volume 4, Proceedings of the VIIth International Congress on Photosynthesis Providence, Rhode Island, USA, August 10–15, 1986. Dordrecht: *Springer Netherlands*, 1987

36. Damour G, Simonneau T, Cochard H, Urban L. An overview of models of stomatal conductance at the leaf level. *Plant, Cell & Environment*, 2010, **33**(9): 1419–1438
37. Ye Z, Yu Q. Mechanism model of stomatal conductance. *Acta Phytoecologica Sinica*, 2009, **33**(4): 772−782 (in Chinese)
38. Blatt M R, Jezek M, Lew V L, Hills A. What can mechanistic models tell us about guard cells, photosynthesis, and water use efficiency. *Trends in Plant Science*, 2022, **27**(2): 166–179
39. Bonan G B. Land-atmosphere CO_2 exchange simulated by a land surface process model coupled to an atmospheric general circulation model. *Journal of Geophysical Research*, 1995, **100**(D2): 2817–2831
40. Sellers P J, Dickinson R E, Randall D A, Betts A K, Hall F G, Berry J A, Collatz G J, Denning A S, Mooney H A, Nobre C A, Sato N, Field C B, Henderson-Sellers A. Modeling the exchanges of energy, water, and carbon between continents and the atmosphere. *Science*, 1997, **275**(5299): 502–509
41. Wang D, Lebauer D, Kling G, Voigt T, Dietze M C. Ecophysiological screening of tree species for biomass production: trade-off between production and water use. *Ecosphere*, 2013, **4**(11): 138
42. Srivastava R K, Panda R K, Chakraborty A, Halder D. Comparison of actual evapotranspiration of irrigated maize in a sub-humid region using four different canopy resistance based approaches. *Agricultural Water Management*, 2018, **202**(1): 156–165
43. Yan H, Yu J, Zhang C, Wang G, Huang S, Ma J. Comparison of two canopy resistance models to estimate evapotranspiration for tea and wheat in southeast China. *Agricultural Water Management*, 2021, **245**: 106581
44. Bittelli M, Ventura F, Campbell G S, Snyder R L, Gallegati F, Pisa P R. Coupling of heat, water vapor, and liquid water fluxes to compute evaporation in bare soils. *Journal of Hydrology*, 2008, **362**(3–4): 191–205
45. Yu L, Zeng Y, Su Z, Cai H, Zheng Z. The effect of different evapotranspiration methods on portraying soil water dynamics and et partitioning in a semi-arid environment in Northwest China. *Hydrology and Earth System Sciences*, 2016, **20**(3): 975–990
46. Zeng Y, Su Z, Wan L, Wen J. A simulation analysis of the advective effect on evaporation using a two-phase heat and mass flow model. *Water Resources Research*, 2011, **47**(10): 2011WR010701
47. Zeng Y, Su Z, Wan L, Wen J. Numerical analysis of air-water-heat flow in unsaturated soil: Is it necessary to consider airflow in land surface models. *Journal of Geophysical Research*, 2011, **116**(D20): D20107
48. Saito H, Šimůnek J, Mohanty B P. Numerical analysis of coupled water, vapor, and heat transport in the vadose zone. *Vadose Zone Journal*, 2006, **5**(2): 784–800
49. Kang S, Gu B, Du T, Zhang J. Crop coefficient and ratio of transpiration to evapotranspiration of winter wheat and maize in a semi-humid region. *Agricultural Water Management*, 2003, **59**(3): 239–254
50. Wang J, Cai H, Kang Y, Chen F. Ratio of soil evaporation to the evapotranspiration for summer maize field. *Transactions of the Chinese Society of Agricultural Engineering*, 2007, **23**(4): 17−22 (in Chinese)
51. Zhang B, Liu Y, Xu D, Cai J, Zhao N. Estimation of summer corn canopy conductance by scaling up leaf stomatal conductance. *Transactions of the Chinese Society of Agricultural Engineering*, 2011, **27**(5): 80−86 (in Chinese)
52. Wang Y, Zeng Y, Yu L, Yang P, Van Der Tol C, Yu Q, Lü X, Cai H, Su Z. Integrated modeling of canopy photosynthesis, fluorescence, and the transfer of energy, mass, and momentum in the soil-plant-atmosphere continuum (STEMMUS-SCOPE v1.0.0). *Geoscientific Model Development*, 2021, **14**(3): 1379–1407
53. Allen R G, Pereira L S, Raes D, Smith M. Crop evapotranspiration: guidelines for computing crop water requirements. Rome: *FAO*, 1998
54. Feddes R A, Kowalik P J, Zaradny H. Simulation of Field Water use and Crop Yield. Wageningen: *Centre for Agricultural Publishing and Documentation*, 1978
55. Šimůnek J J, Šejna M, Saito H, Sakai M, van Genuchten M. The HYDRUS-1D software package for simulating the one-dimensional movement of water, heat, and multiple solutes in variably-saturated media. Riverside, California: *Department of Environmental Sciences, University of California Riverside*, 2008
56. van de Griend A A, Owe M. Bare soil surface resistance to evaporation by vapor diffusion under semiarid conditions. *Water Resources Research*, 1994, **30**(2): 181–188
57. European Centre for Medium-Range Weather Forecasts (ECMWF). IFS Documentation CY48R1 - Part IV: Physical Processes. *ECMWF*, 2023
58. Katerji N, Perrier A, Renard D, Aissa A K O. A model of actual evapotranspiration (ETR) for a field of lucerne: the role of a crop coefficient. *Agronomie*, 1983, **3**(6): 513−521 (in French)
59. Massman W J. A surface energy balance method for partitioning evapotranspiration data into plant and soil components for a surface with partial canopy cover. *Water Resources Research*, 1992, **28**(6): 1723–1732
60. Kelliher F M, Leuning R, Raupach M R, Schulze E D. Maximum conductances for evaporation from global vegetation types. *Agricultural and Forest Meteorology*, 1995, **73**(1–2): 1–16
61. Ortega-Farias S, Olioso A, Antonioletti R, Brisson N. Evaluation of the Penman-Monteith model for estimating soybean evapotranspiration. *Irrigation Science*, 2004, **23**(1): 1–9
62. Gharsallah O, Facchi A, Gandolfi C. Comparison of six evapotranspiration models for a surface irrigated maize agro-ecosystem in Northern Italy. *Agricultural Water Management*, 2013, **130**: 119–130

63. Wei Z, Paredes P, Liu Y, Chi W W, Pereira L S. Modelling transpiration, soil evaporation and yield prediction of soybean in North China Plain. *Agricultural Water Management*, 2015, **147**: 43–53
64. Zhao N, Liu Y, Cai J, Paredes P, Rosa R D, Pereira L S. Dual crop coefficient modelling applied to the winter wheat-summer maize crop sequence in North China Plain: basal crop coefficients and soil evaporation component. *Agricultural Water Management*, 2013, **117**: 93–105
65. Harris P P, Huntingford C, Cox P M, Gash J H C, Malhi Y. Effect of soil moisture on canopy conductance of Amazonian rainforest. *Agricultural and Forest Meteorology*, 2004, **122**(3-4): 215–227
66. Wang Y, Horton R, Xue X, Ren T. Partitioning evapotranspiration by measuring soil water evaporation with heat-pulse sensors and plant transpiration with sap flow gauges. *Agricultural Water Management*, 2021, **252**: 106883
67. Li X, Kang S, Li F, Jiang X, Tong L, Ding R, Li S, Du T. Applying segmented Jarvis canopy resistance into Penman-Monteith model improves the accuracy of estimated evapotranspiration in maize for seed production with film-mulching in arid area. *Agricultural Water Management*, 2016, **178**: 314–324
68. Wu Z, Cui N, Zhao L, Han L, Hu X, Cai H, Gong D, Xing L, Chen X, Zhu B, Lv M, Zhu S, Liu Q. Estimation of maize evapotranspiration in semi-humid regions of northern China using Penman-Monteith model and segmentally optimized Jarvis model. *Journal of Hydrology*, 2022, **607**: 127483